Ultramicroscopy 132 (2013) 212–215

Contents lists available at ScienceDirect

Ultramicroscopy

journal homepage: www.elsevier.com/locate/ultramic

Phase separation in equiatomic AlCoCrFeNi high-entropy alloy

A. Manzoni [a,*], H. Daoud [b], R. Völkl [b], U. Glatzel [b], N. Wanderka [a]

[a] Helmholtz-Zentrum Berlin, Institute of Applied Materials, D-14109 Berlin, Germany
[b] Metals and Alloys, University Bayreuth, Ludwig-Thoma-Strasse 36b, D-95447 Bayreuth, Germany

ARTICLE INFO

Available online 20 December 2012

Keywords:
High entropy alloys
Atom probe tomography
Phase separation
Spinodal decomposition

ABSTRACT

The microstructure of the as-cast AlCoCrFeNi high entropy alloy has been investigated by transmission electron microscopy and atom probe tomography. The alloy shows a very pronounced microstructure with clearly distinguishable dendrites and interdendrites. In both regions a separation into an Al–Ni rich matrix and Cr–Fe-rich precipitates can be observed. Moreover, fluctuations of single elements within the Cr–Fe rich phase have been singled out by three dimensional atom probe measurements. The results of investigations are discussed in terms of spinodal decomposition of the alloying elements inside the Cr–Fe-rich precipitates.

1. Introduction

High-entropy alloys have been known for some years as a new class of materials, which is defined ideally as a solid solution of five or more elements, each being present with 5–35 at% [1–5]. Another criterion for the definition, beside of course the high-entropy, is the small difference in atomic radii δ of the constituting elements, which should be $\delta \leq 6.6\%$ [6]. δ has been defined as

$$\delta = \sqrt{\sum_{i=1}^{n} c_i \left(1 - \frac{r_i}{\bar{r}}\right)^2}$$

where c_i is the atomic percentage of the ith component, $\bar{r} = \sum_{i=1}^{n} c_i r_i$ is the average atomic radius and r_i is the atomic radius [7].

The most studied alloy is the as-cast equiatomic AlCoCrCuFeNi alloy, which stands out by its interesting thermomechanic properties such as high hardness, resistance to softening at high temperatures and good compressive strength [8,9]. As the mechanical properties depend highly on the microstructure, the latter was studied intensively in order to understand the macroscopic behavior. The as-cast equiatomic AlCoCrCuFeNi alloy contains mainly Al–Ni- and Cr–Fe-rich phases with bcc structures, the Al–Ni-rich phase being an ordered phase of B2 type and the Cr–Fe-rich phase being a disordered phase [10]. In addition, several Cu-rich phases were detected. Detailed investigations on the Cu-rich phases can be found in recently published work [10]. The knowledge of the microstructure can e.g. explain the ferromagnetic behavior in this type of alloys, as has been shown recently [11].

In order to inhibit the formation of Cu-rich phases at the grain boundaries and inside the grains and thus reduce the number of phases, this element has been omitted in this alloy. In the literature there is only little information about the microstructure of the 5 component equiatomic AlCoCrFeNi alloy [4,12–14]. Wang et al. [13] showed that the alloy solidifies into dendrites and interdendrites, both of which show a separation into two or three phases. However, no information is available on a nanometer level, which is why this alloy has been studied in detail by transmission electron microscopy (TEM) and three dimensional atom probe (3D-AP) in the present study.

2. Materials and methods

All alloying elements with 99.999% purity were melted in an equiatomic ratio in an induction levitation furnace under argon atmosphere. The produced ingots were remelted several times in order to ensure homogeneity and then cooled inside the furnace.

Specimens for investigation by light microscope were etched with a solution of molybdenum acid with H_2O, HCl and HNO_3. Samples for TEM observations were prepared in two steps, first by mechanical grinding down to a thickness of 10 μm, and second by argon milling down to electron transparency. The TEM that was used for this study was a Philips CM 30, operated at 300 kV. It is equipped with an energy-dispersive X-ray spectrometer (EDX) which has been used for microchemical observations.

A focused ion beam (FIB, ZEISS 1540 EsB Crossbeam®) operated at 30 kV, has been used for the 3D-reconstruction of the phases in the alloy. Images have been taken with a secondary electron detector while subsequently cutting new sections by

* Corresponding author. Tel.: +49 30806242326; fax: +49 30806243059.
E-mail address: anna.manzoni@helmholtz-berlin.de (A. Manzoni).

0304-3991/$ - see front matter © 2012 Elsevier B.V. All rights reserved.
http://dx.doi.org/10.1016/j.ultramic.2012.12.015

gallium ions with a beam current of 50 pA, which induces a milling step in the *z*-direction of ~13 nm. The 3D reconstruction has been done with the software "Avizo Fire 7.0.1".

Rods of $0.25 \times 0.25 \times 10\ mm^3$ were cut from the ingot and polished mechanically down to a tip radius of ~2 μm for micro-chemical studies in a 3D-AP. They were subsequently polished down to a tip diameter of ~100 nm by annular milling with gallium ions in the FIB, operated at 30 kV with beam currents from 2 nA in the beginning down to 10 pA for the final polishing. The 3D-AP (CAMECA) was operated with a pulse fraction of 20% and a pulse penetration frequency of 1000 Hz. 7 samples were investigated in a vacuum of better than 10^{-7} Pa at a temperature of 70 K.

3. Results and discussion

The etched samples were investigated by light microscope and they show very large grains up to 1 mm in length (not shown here). A pronounced dendritic solidification as shown in Fig. 1 can be seen in every grain. Dendrites as well as interdendrites contain the same phases, namely Cr–Fe-rich precipitates embedded in an Al–Ni-rich matrix. Whereas the bright interdendrites are characterized by an intertwined structure where Al–Ni- and Cr–Fe rich phases alternate with a period of ~100 nm in the width (see Fig. 2a) the dark contrasted dendrites are characterized by Cr–Fe-rich precipitates of cuboidal morphology (see Fig. 2b). The observed microstructure of the interdendrites is different from that of the 6 component equiatomic AlCoCrCuFeNi alloy [10]. The existence of Cu in the 6 component equiatomic alloy leads to the formation of a single Cu-rich interdendritic phase [10]. However, in the interdendrites of the 5 component equiatomic alloy two phases can be observed, each one with a similar composition to those in the dendrites.

In the following, the present work concentrates on the microstructure investigations in the dendrites only. A bright field TEM micrograph (Fig. 2b) shows the presence of a dark Al–Ni-rich matrix indicated by **A** and Cr–Fe-rich precipitates indicated by **B**. The selected area diffraction (SAD) pattern shows that the matrix has a B2 structure. The bright roundish, about 25–100 nm wide precipitates have a disordered bcc structure. The structures of the phases obtained in the 5 component equiatomic alloy are the same as those of the 6 component alloy [10]. Fig. 3 visualizes the morphology of Cr–Fe-rich precipitates by FIB tomography. The 3D reconstruction reveals that the Cr–Fe-rich precipitates are not interconnected, which is made more visible by using different colors for the individual precipitates. Their volume percent in the Al–Ni-rich matrix is ~30% according to the calculation by Avizo

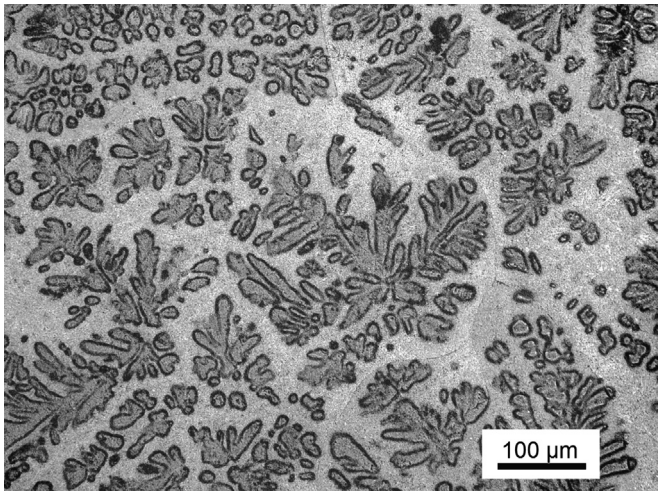

Fig. 1. Optical micrograph of the AlCoCrFeNi alloy. Dendrites are imaged dark and the interdendrites bright.

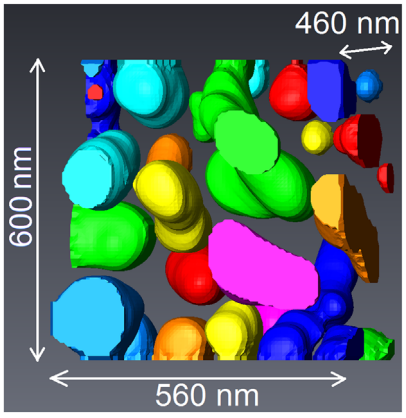

Fig. 3. Visualization of the individual Cr–Fe rich precipitates by FIB tomography in a volume of $600 \times 560 \times 460\ nm^3$.

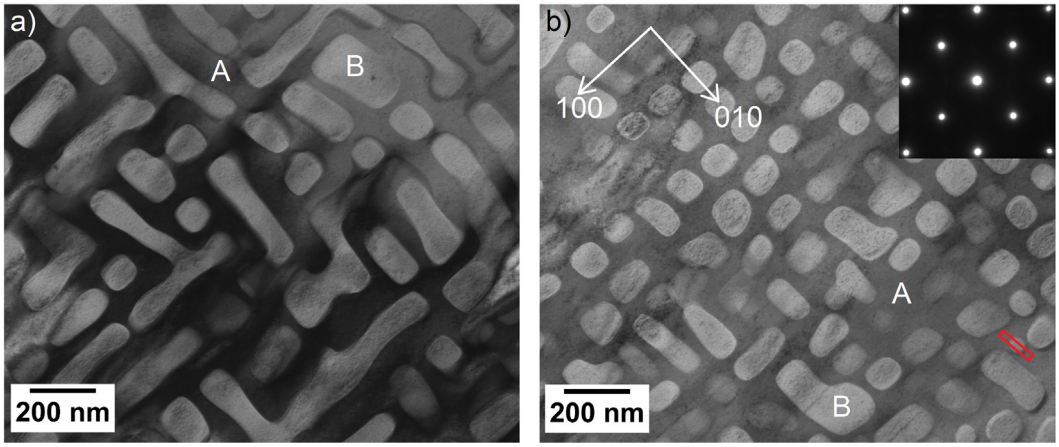

Fig. 2. BF TEM images of the microstructure of the as-cast AlCoCrFeNi alloy: (a) interdendrites and (b) dendrites. The corresponding selected area electron diffraction pattern of the [001] zone axis of bcc structure is shown in the inset of (b). The matrix indicated by **A** is Al–Ni rich. The bright precipitates indicated by **B** are Cr–Fe-rich. The red box corresponds to a region where the investigated sample from Fig. 4 could have been taken. (For interpretation of the references to colour in this figure legend, the reader is referred to the web version of this article.)

Table 1
Microchemical composition of the investigated areas of the AlCoCrFeNi alloy. A and B have been determined by TEM/EDX measurements, 1–3 by 3D–AP. The relative error is given by the standard deviation 2σ.

Symbols	Regions enriched	Al [at%]	Co [at%]	Cr [at%]	Fe [at%]	Ni [at%]
A	Al–Ni	32.0 ± 3.4	22.6 ± 2.0	4.9 ± 1.4	13.0 ± 1.1	27.5 ± 2.6
B	Cr–Fe	4.9 ± 3.6	22.3 ± 0.6	35.7 ± 5.1	29.9 ± 2.1	7.7 ± 3.4
1	Al–Ni	31.5 ± 3.5	19.6 ± 1.9	3.7 ± 0.7	13.1 ± 1.6	32.0 ± 2.1
2	Cr–Fe	8.5 ± 1.4	19.2 ± 1.5	35.7 ± 5.3	27.0 ± 0.4	9.4 ± 1.9
2a	Fe–enriched	5.8 ± 1.0	24.6 ± 6.4	15.3 ± 5.8	47.1 ± 3.4	7.0 ± 2.1
2b	Cr–enriched	7.1 ± 2.8	14.0 ± 1.4	50.1 ± 1.8	21.8 ± 1.7	6.8 ± 1.5
3	Al–Ni without Co	35.9 ± 0.3	6.9 ± 0.2	1.9 ± 0.1	3.3 ± 0.1	51.9 ± 0.3
3a	Al–enriched	50.8 ± 2.1	4.6 ± 1.4	2.8 ± 1.3	5.5 ± 1.1	36.1 ± 1.7
3b	Ni–enriched	7.3 ± 2.3	3.6 ± 0.8	0.9 ± 0.7	4.3 ± 1.5	83.9 ± 1.8

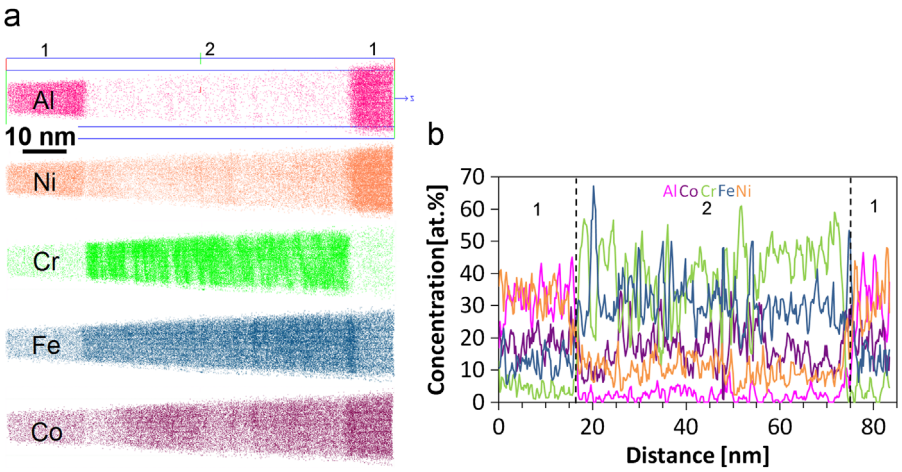

Fig. 4. (a) Three dimensional reconstruction of Al, Co, Cr Fe and Ni atom positions in an investigated volume of $13 \times 13 \times 83$ nm^3 of the AlCoCrFeNi as-cast alloy and (b) the concentration depth profiles of all alloying elements taken along a cylinder of 1 nm in radius placed in the middle axis of the investigated volume in (a).

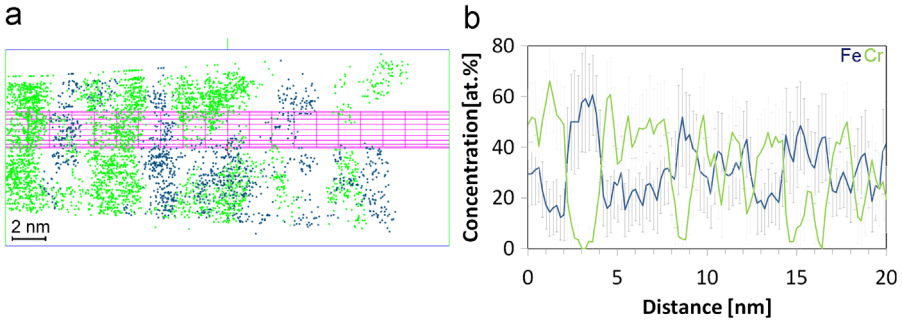

Fig. 5. (a) Three dimensional reconstruction of Fe-clusters (threshold $>40\%$), in blue, and Cr-clusters (threshold $>45\%$), in green, and (b) the corresponding concentration depth profiles for Fe and Cr, taken along the cylinder defined in (a). (For interpretation of the references to color in this figure legend, the reader is referred to the web version of this article.)

Fire 7.0.1. The Al–Ni rich matrix has not been visualized here. It can be concluded that the Cr–Fe-rich phase is more pronounced in the interdendritic region, which is indeed the case (see Fig. 2a). Its volume percent has been found to be $\sim$52%. The composition of both phases has been determined by TEM–EDX and is given in Table 1. The compositions of the two phases correspond sensibly to the corresponding ones observed in the equiatomic AlCoCrCuFeNi alloy, given in [10].

Microchemical information on a nanometer scale has been obtained by three dimensional atom probe measurements. Fig. 4 shows the 3D reconstruction of all alloying elements in an investigated volume of $13 \times 13 \times 83$ nm^3 and the concentration depth profiles taken along a cylinder of 1 nm in radius which was located in the z-axis of the specimen (not shown here). The investigated sample is characterized by a non-uniform distribution of all alloying elements and a correlation between Al and Ni on the one hand and Fe and Cr on the other hand. Two regions, labeled 1 and 2, can be distinguished both in the 3D reconstruction and in the concentration depth profiles. Region 1 is Al–Ni-rich, whereas region 2 is Cr–Fe-rich:

(a) Al–Ni rich region
Region 1 shows quite a homogeneous distribution of the elements and will not be examined in detail, because it corresponds well to the Al–Ni rich phases observed in the 6 component AlCoCrCuFeNi alloy [10]. The average composition of this region is given in Table 1. When comparing the composition of the Al–Ni-rich phase in both the 5 and 6 component equiatomic alloys it is obvious that within the error bars it is similar.

(b) Cr–Fe-rich region
Unlike the Al–Ni rich phase, the Cr–Fe-rich phase in this alloy is characterized by contents of Al, Fe and Ni that differ strongly from those in the 6 component alloy [10]. Fig. 5a shows the reconstruction of Fe- and Cr-rich clusters in region 2 from Fig. 4b, defined by thresholds of $>40\%$ for Fe clusters and of $>45\%$ for Cr clusters. The concentration depth profiles along a cylinder of 1 nm in radius (Fig. 5a) for the elements Fe and Cr are shown in Fig. 5b. The other elements have been omitted for the sake of clarity. The definition of the Fe- and Cr-rich clusters and their concentration in Fe and Cr are regrouped in Table 1 as 2a and 2b, respectively. An alternation of Fe- and Cr-rich clusters is visible in Fig. 5a. It should be mentioned that a reconstruction of Fe- and Cr- iso-surfaces representing the same amount of Fe and Cr like in the clusters (not shown here) indicates that these two types of clusters are highly intertwined.
Strong anti-correlated fluctuations of Fe- and Cr-atoms can be observed over the whole concentration depth profiles (Fig. 5b). In regions of about 2 nm width the local Fe or Cr concentration can climb up to about 55 at% for both elements or fall down to about 5 at% in the case of Cr and about 25 at% in the case of Fe. These opposite fluctuations, as well as the highly intertwined morphology, have been observed in previous [11,15] and have been attributed to the spinodal decomposition of Fe- and Cr-rich phases. The amplitude of the fluctuations is more pronounced in the present AlCoCrFeNi alloy than in the equiatomic AlCoCrCuFeNi alloy. This difference might be due to the absence of Cu in the present alloy.

4. Summary

The combined TEM and 3D-AP investigations of the equiatomic AlCoCrFeNi high-entropy alloy demonstrate the following:

(a) The alloy decomposes into dendrites and interdendrites which contain the same phases, namely Cr–Fe-rich precipitates embedded in an Al–Ni-rich matrix.
(b) The Al–Ni rich matrix shows quite a homogeneous distribution of all alloying elements, and it corresponds well to the Al–Ni rich phases investigated in the 6 component equiatomic alloy.
(c) The Cr–Fe-rich precipitates show a small scale decomposition within the phase. Anti-correlated fluctuations of Fe- and Cr-rich domains have been attributed to the spinodal decomposition.

Acknowledgment

The authors are grateful to the German Research foundation (DFG) for the financial support by WA 1378/15-1 and GL 181/25-1. The authors would like to thank Ch. Förster for sample preparation and H. Kropf for help with FIB-tomography.

References

[1] J.W. Yeh, S.K. Chen, S.J. Lin, J.Y. Gan, T.S. Chin, T.T. Shun, C.H. Tsau, S.Y. Chang, Nanostructured high-entropy alloys with multiple principal elements: Novel alloy design concepts and outcomes, Advanced Engineering Materials 6 (2004) 299–303.
[2] B. Cantor, I.T.H. Chang, P. Knight, A.J.B. Vincent, Microstructural development in equiatomic multicomponent alloys, Materials Science and Engineering A 375 (2004) 213–218.
[3] C.C. Tung, J.W. Yeh, T.T. Shun, S.K. Chen, Y.S. Huang, H.C. Chen, On the elemental effect of AlCoCrCuFeNi high-entropy alloy system, Materials Letters 61 (2007) 1–5.
[4] C.M. Lin, H.L. Tsai, Evolution of microstructure, hardness, and corrosion properties of high-entropy Al(0.5)CoCrFeNi alloy, Intermetallics 19 (2011) 288–294.
[5] C.J. Tong, Y.L. Chen, S.K. Chen, J.W. Yeh, T.T. Shun, C.H. Tsau, S.J. Lin, S.Y. Chang, Microstructure characterization of AlxCoCrCuFeNi high-entropy alloy system with multiprincipal elements, Metallurgical and Materials Transactions A 36A (2005) 881–893.
[6] X. Yang, Y. Zhang, Prediction of high-entropy stabilized solid-solution in multi-component alloys, Materials Chemistry and Physics 132 (2012) 233–238.
[7] C. Kittel, Einführung in die Festkörperphysik, 14 ed., Oldenbourg Wissenschaftsverlag GmbH, 2006.
[8] C.J. Tong, M.R. Chen, S.K. Chen, J.W. Yeh, T.T. Shun, S.J. Lin, S.Y. Chang, Mechanical performance of the AlxCoCrCuFeNi high-entropy alloy system with multiprincipal elements, Metallurgical and Materials Transactions A 36A (2005) 1263–1271.
[9] J.W. Yeh, Y.L. Chen, S.J. Lin, S.K. Chen, High-entropy alloys—a new era of exploitation, in: H.B. Ramirez, J.G. Cabanas-Moreno, H.A. Calderon-Benavides, K. Ishizaki, A. Salinas-Rodriguez (Eds.), Advanced Structural Materials, vol. III, 2007, pp. 1–9.
[10] S. Singh, N. Wanderka, B.S. Murty, U. Glatzel, J. Banhart, Decomposition in multi-component AlCoCrCuFeNi high-entropy alloy, Acta Materialia 59 (2011) 182–190.
[11] S. Singh, N. Wanderka, K. Kiefer, K. Siemensmeyer, J. Banhart, Effect of decomposition of the Cr–Fe–Co rich phase of AlCoCrCuFeNi high entropy alloy on magnetic properties, Ultramicroscopy 111 (2011) 619–622.
[12] T.T. Shun, Y.C. Du, Microstructure and tensile behaviors of FCC Al(0.3)CoCrFeNi high entropy alloy, Journal of Alloys and Compounds 479 (2009) 157–160.
[13] Y.P. Wang, B.S. Li, M.X. Ren, C. Yang, H.Z. Fu, Microstructure and compressive properties of AlCrFeCoNi high entropy alloy, Materials Science and Engineering A 491 (2008) 154–158.
[14] T.T. Shun, C.H. Hung, C.F. Lee, The effects of secondary elemental Mo or Ti addition in Al(0.3)CoCrFeNi high-entropy alloy on age hardening at 700 °C, Journal of Alloys and Compounds 495 (2010) 55–58.
[15] M.K. Miller, J.M. Hyde, M.G. Hetherington, A. Cerezo, G.D.W. Smith, C.M. Elliott, Spinodal deomposition in Fe–Cr alloys—Experimental study at the atomic level and comparison with computer models. 1. Introduction and methodology, Acta Metallurgica et Materialia 43 (1995) 3385–3401.